Trajectory Design for a Solar Sail Mission to Asteroid 2016 HO3

Heiligers, Jeannette; Fernandez, Juan M.; Stohlman, Olive R.; Wilkie, W. Keats

Publication date
2018

Document Version
Accepted author manuscript

Published in
Proceedings of the AAS/AIAA Astrodynamics Specialist Conference

Citation (APA)
Heiligers, J., Fernandez, J. M., Stohlman, O. R., & Wilkie, W. K. (2018). Trajectory Design for a Solar Sail Mission to Asteroid 2016 HO3. In *Proceedings of the AAS/AIAA Astrodynamics Specialist Conference* Article AAS-18-314

AAS-18-314

TRAJECTORY DESIGN FOR A SOLAR-SAIL MISSION TO ASTEROID 2016 HO_3

Jeannette Heiligers*, Juan M. Fernandez†, Olive R. Stohlman†, and W. Keats Wilkie†

This paper proposes the use of solar-sail technology currently under development at NASA Langley Research Center for a CubeSat rendezvous mission with asteroid 2016 HO_3, a quasi-satellite of Earth. Time-optimal trajectories are sought for within a 2022 – 2023 launch window, starting from an assumed launcher ejection condition in the Earth-Moon system. The optimal control problem is solved through a particular implementation of a direct pseudo-spectral method for which initial guesses are generated through a relatively simple and straightforward genetic algorithm search on the optimal launch date and sail attitude. The results show that the trajectories take 2.16 – 4.21 years to complete, depending on the assumed solar-sail reflectance model and solar-sail technology. To assess the performance of solar-sail propulsion for this mission, the trajectory is also designed assuming the use of near-term solar electric propulsion. The resulting fuel-optimal trajectories take longer to complete than the solar-sail trajectories and require a propellant consumption that exceeds the expected propellant capacity onboard the CubeSat. This comparison demonstrates the superior performance of solar-sail technology for this mission.

INTRODUCTION

On 27 April 2016, the Pan-STARRS 1 asteroid survey telescope on Haleakalā, Hawaii, detected a remarkable asteroid: 2016 HO_3.‡ Its orbit is extremely similar to that of Earth, to the extent that asteroid 2016 HO_3 appears to orbit around our planet. The asteroid is therefore considered a near-Earth companion or a quasi-satellite of Earth and is expected to accompany the Earth for hundreds of years.‡ This unique characteristic, together with the already significant increase in interest in small-body research over recent years, makes 2016 HO_3 an interesting mission target.

* Delft University of Technology, Faculty of Aerospace Engineering, Kluyverweg 1, 2629 HS Delft, the Netherlands

† National Aeronautics and Space Administration, Langley Research Center, Structural Dynamics Branch, Hampton, Virginia, 23681-2199, USA

‡ Jet Propulsion Laboratory, "Small Asteroid Is Earth's Constant Companion", https://www.jpl.nasa.gov/news/news.php?feature=6537, Accessed 19 February 2018.

Even though the orbit of 2016 HO_3 is very similar to that of Earth, its phasing and the 7.8 deg inclination with respect to the ecliptic makes it a difficult target to reach. Low-thrust propulsion, either in the form of solar electric propulsion (SEP) or solar sailing,[1, 2] has been proven to enable high-energy missions. Examples for the use of SEP include JAXA's asteroid sample return mission Hayabusa,[3] NASA's Dawn mission that visited the two largest bodies in the asteroid belt,[4] and ESA's planned BepiColombo mission to Mercury.[5] Examples of proposed high-energy solar-sail missions include NASA's NEA Scout mission,[6] as well as a range of theoretical mission concepts such as the Solar Polar Orbiter,[7] the Geostorm mission concept,[8, 9] the Interstellar Heliopause Probe,[10] and, more generally, a wide range of highly non-Keplerian orbits for novel space applications.[1, 11-16]

This paper investigates the use of solar-sail propulsion to rendezvous with asteroid 2016 HO_3. In particular, the solar-sail technology currently under development at NASA Langley Research Center is considered.[17] The assumed mission configuration is that of a CubeSat platform and a launch as secondary payload (e.g., onboard one of the Exploration Missions of the SLS launch vehicle) within a wide 2022 – 2023 launch window. The assumption of a CubeSat-sized platform drove the choice for solar-sail propulsion as mass and dimension constraints limit the available space for SEP propellant as well as solar arrays to provide power to the SEP system. To confirm this choice, the trajectory will not only be designed for the use of solar-sail propulsion, but also for the use of solar electric propulsion.

The objective of the work in this paper is to find time-optimal solar-sail – or alternatively fuel-optimal SEP - trajectories from an assumed launcher ejection condition in the Earth-Moon circular restricted three-body problem (CR3BP) to 2016 HO_3. An initial, ballistic trajectory up to the sphere of influence of the Earth is assumed to allow spacecraft testing and verification. Once at the sphere of influence, the low-thrust propulsion system is activated and the modelling of the trajectory continues in the Sun-Earth CR3BP. Time- and fuel-optimal trajectories are found through the application of a specific direct pseudospectral optimal control solver, PSOPT.[18] Initial guesses for the optimal control solver are obtained through a relatively straightforward genetic algorithm routine that finds the optimal launch date and *constant* direction of the low-thrust acceleration vector with respect to the direction of sunlight to minimize the miss-distance and miss-velocity at the asteroid. By subsequently feeding this initial guess to the optimal control solver, where the control is allowed to vary over time, these errors are overcome and the time of flight – or alternatively the fuel consumption - is minimized.

ORBIT OF 2016 HO_3

The orbital elements of asteroid 2016 HO_3 are provided in Table 1. With a semi-major axis very close to that of Earth and only a small eccentricity, its orbit resembles that of Earth (only inclined at 7.8 deg with respect to the ecliptic). Graphical representations of the asteroid's motion in the timeframe 1960 – 2020 appear in Figure 1, where the Earth is assumed to be on a Keplerian, 1 AU (astronomical unit) circular orbit. Figure 1a shows the orbit in an inertial frame, $A(X_I, Y_I, Z_I)$, where the X_I-axis points towards the vernal equinox, the Z_I-axis is oriented perpendicular to the ecliptic and the Y_I-axis completes the right-handed reference frame. Instead, Figure 1b shows the orbit in a synodic frame, $B_{SE}(x_{SE}, y_{SE}, z_{SE})$, centered at the Sun-Earth barycenter where the x_{SE}-axis points along the Sun-Earth line, the z_{SE}-axis is oriented perpendicular to the ecliptic plane and the y_{SE}-axis completes the right-handed reference frame. This frame thus rotates with the Earth's motion around the Sun. The side-view plots in the bottom row of Figure 1 clearly show the asteroid's 7.8 deg inclination with respect to the ecliptic.

Table 1. Orbital elements of 2016 HO_3 (source: JPL Small-Body Database Browser*).

Orbital element	Value
Semi-major axis, a	1.0014 AU
Eccentricity, e	0.1040
Inclination, i	7.7741 deg
Right ascension of the ascending node, Ω	66.4066 deg
Argument of perihelion, ω	306.9337 deg

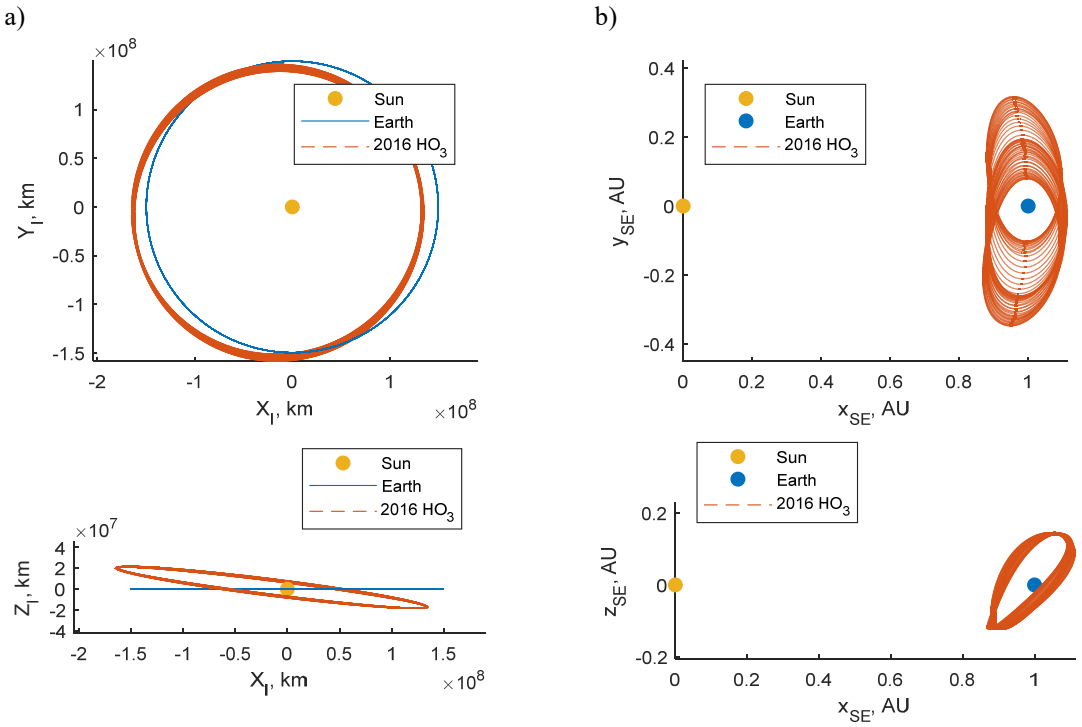

Figure 1. Orbit of 2016 HO_3 in the 1960 – 2020 timeframe.
a) In the inertial frame $A(X_I, Y_I, Z_I)$. b) In the synodic Sun-Earth frame $B_{SE}(x_{SE}, y_{SE}, z_{SE})$.

SOLAR-SAIL TECHNOLOGY

The solar-sail architectures assumed for this study are based upon small satellite solar-sail systems and technologies now under development at NASA Langley Research Center (NASA LaRC).[17] These solar-sail systems are based upon new deployable composite boom technologies being developed by LaRC and the

* Jet Propulsion Laboratory, "JPL Small-Body Database Browser", https://ssd.jpl.nasa.gov/sbdb.cgi, Accessed 19 December 2017

German Aerospace Center (DLR) specifically for small satellites.* In 2016, NASA LaRC built and ground-tested a 9.2 m by 9.2 m composites-based engineering development unit (EDU) solar-sail system suitable for 6U CubeSat spacecraft. This EDU solar-sail system stowed within a 20 cm x 10 cm x 15 cm volume inside the 6U CubeSat chassis. This system was initially conceived as a risk-reducing alternative to NASA's Near Earth Asteroid (NEA) Scout solar-sail baseline design, which used open cross-section metallic *triangular rollable and collapsible* (TRAC) booms.[6,23] TRAC boom solar-sail designs have been used on smaller solar sail demonstration flights, most notably with the NASA NanoSail D2 solar sail, and the Planetary Society LightSail 1 (formerly, LightSail A) and LightSail 2 solar sails.[24] TRAC booms have been problematic for larger solar sails due to their high coefficient of thermal expansion (CTE), very low torsional stiffness, and low deployed precision.[25,26] An improved version of the composites-based EDU solar sail – the Advanced Composites-Based Solar Sail System (ACS3) - is now under development by NASA LaRC and NASA Ames Research Center for a low Earth orbit (LEO) solar sail technology risk reduction mission in the 2021 timeframe. The 6U ACS3 flight experiment is intended as a technology development pathfinder for a future, larger composites-based small satellite solar-sail system suitable for 12U to 27U CubeSat class spacecraft. For purposes of this study, a lightness number range bounding the anticipated solar sail performance of a notional 12U-27U CubeSat-class spacecraft using the ACS3 solar sail technology is assumed.

MISSION ASSUMPTIONS

To design the trajectory from launch ejection to 2016 HO_3, a set of assumptions are made:

- Launch is assumed to take place in 2022 – 2023
- The trajectory is assumed to start from the following dimensional initial state in a synodic Earth-Moon frame $B_{EM}\left(x_{EM}, y_{EM}, z_{EM}\right)$ with $\mathbf{r}_0$ the initial position vector in km and $\mathbf{V}_0$ the initial velocity vector in km/s:

$$\mathbf{x}_0 = \begin{bmatrix} \mathbf{r}_0 \\ \mathbf{V}_0 \end{bmatrix} = \begin{bmatrix} 26503.0 \\ -371.3 \\ 9134.6 \\ 4.43 \\ 2.41 \\ 0.85 \end{bmatrix}. \tag{1}$$

  Note that frame $B_{EM}\left(x_{EM}, y_{EM}, z_{EM}\right)$ is centered at the Earth-Moon barycenter with the x_{EM}-axis pointing to the Moon, the z_{EM}-axis perpendicular to the Earth-Moon orbital plane, and the y_{EM}-axis completing the right-handed frame. The state vector in Eq. (1) corresponds to a spacecraft-Earth distance of 32,486 km and an inertial velocity with respect to Earth of 5.16 km/s (the local escape velocity is 4.95 km/s).
- Starting from the initial state in Eq. (1), a ballistic arc up to the Earth's sphere of influence (SOI) is assumed after which the solar sail or SEP system is activated to rendezvous with 2016 HO_3.

---

* NASA Game Changing Development Program, "Deployable Composite Booms (DCB)", https://gameon.nasa.gov/projects/deployable-composite-booms-dcb/ Accessed 10 August, 2018.

- The trajectory propagation up to the Earth's SOI is assumed to take place in the Earth-Moon CR3BP, while the subsequent propelled phase is assumed to take place in the Sun-Earth CR3BP. When linking these CR3BPs and when computing the orbit of 2016 HO_3 in the Sun-Earth CR3BP the following is assumed for the ephemerides of the Earth and Moon:
  - For Earth, a set of analytical ephemerides is used, but the eccentricity is set to zero
  - For the Moon, a set of constant Keplerian elements is used
- Regarding the propulsion system, the following assumptions are made:
  - Solar sail
    - The solar-sail lightness number is assumed to be in the range $\beta = 0.025 - 0.04$ for a 12U – 27U spacecraft (for a definition of the lightness number, see below Eq. (7))
  - It is assumed that the solar-sail system can be replaced by a solar electric propulsion system (and power system) with a performance that is based on the following assumptions
    - An initial spacecraft mass of 14 – 21 kg is assumed
    - A specific impulse of 1,600 s is assumed[19]
    - A maximum thrust of 0.9 mN is assumed[19]
    - A maximum propellant mass capacity of 1.5 kg is assumed[19]
    - A maximum thruster operation duration of 20,000 hours (2.3 years) is assumed[19]

DYNAMICS

As outlined in the previous section, two different sets of dynamical frameworks are adopted to design the trajectory to 2016 HO_3: the Earth-Moon CR3BP from the initial condition in Eq. (1) up to the Earth's SOI (hereafter referred to as the Earth-Moon ballistic phase) and the Sun-Earth CR3BP from the Earth's SOI up to rendezvous with the asteroid (hereafter referred to as the interplanetary phase). The dynamics in both phases will be detailed in the following subsections, starting with the interplanetary phase.

Interplanetary phase

Considering the relatively close proximity of the asteroid to Earth and its semi-bounded motion around Earth as shown in Figure 1b, the trajectory to 2016 HO_3 is designed in the framework of the Sun-Earth CR3BP. In the CR3BP, the motion of an infinitely small mass, m, (i.e., the spacecraft), is described under the influence of the gravitational attraction of two much larger primary masses, m_1 (here, the Sun) and m_2 (here, the Earth). The gravitational influence of the small mass on the primary masses is neglected and the primary masses are assumed to move in circular orbits about their common center-of-mass. The reference frame employed to define the spacecraft's dynamics in the Sun-Earth CR3BP is that of Figure 1b: the synodic Sun-Earth frame $B_{SE}\left(x_{SE}, y_{SE}, z_{SE}\right)$, which rotates at constant angular velocity, ω, about the z-axis, $\boldsymbol{\omega} = \omega\hat{\mathbf{z}}$, see Figure 2.

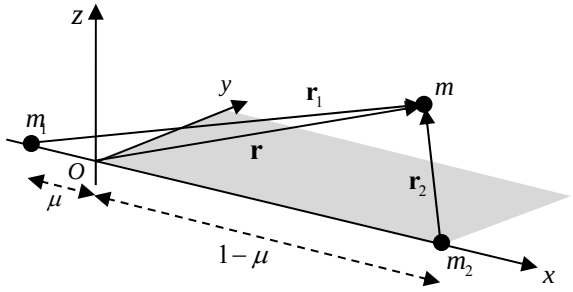

Figure 2. Schematic of circular restricted three-body problem.

New units are introduced: the sum of the two primary masses is taken as the unit of mass, i.e., $m_1 + m_2 = 1$. Then, with the mass ratio $\mu = m_2 / (m_1 + m_2)$, the masses of these primary bodies become $m_1 = 1 - \mu$ and $m_2 = \mu$. As unit of length, the distance between the primary bodies is selected, and $1/\omega$ is chosen as the unit of time, yielding $\omega = 1$. Then, one revolution of the reference frame (i.e., one year for the Sun-Earth CR3BP) is represented by 2π. In this framework, the motion of a low-thrust propelled spacecraft is described by

$$\ddot{\mathbf{r}} + 2\boldsymbol{\omega} \times \dot{\mathbf{r}} + \boldsymbol{\omega} \times (\boldsymbol{\omega} \times \mathbf{r}) = \mathbf{a} - \nabla V \tag{2}$$

with $\mathbf{r} = \begin{bmatrix} x & y & z \end{bmatrix}^T$ the position vector of m.

The terms on the left-hand side of Eq. (2) are the kinematic, coriolis and centripetal accelerations, respectively, while the terms on the right-hand side are the low-thrust acceleration and the gravitational acceleration exerted by the primary masses. In frame $B_{SE}(x_{SE}, y_{SE}, z_{SE})$ the gravitational potential, V, is given by

$$V = -\left(\frac{1-\mu}{r_1} + \frac{\mu}{r_2} \right), \tag{3}$$

where r_1 and r_2 are the magnitudes of the vectors $\mathbf{r}_1 = \begin{bmatrix} x + \mu & y & z \end{bmatrix}^T$ and $\mathbf{r}_2 = \begin{bmatrix} x - (1-\mu) & y & z \end{bmatrix}^T$, respectively, see Figure 2. Finally, the term $\mathbf{a}$ is the low-thrust acceleration vector which in this paper is either provided by a solar sail, $\mathbf{a} = \mathbf{a}_s$, or a solar electric propulsion system, $\mathbf{a} = \mathbf{a}_T$. Its definition therefore depends on the type of low-thrust propulsion system employed which will be discussed separately in the following two subsections.

Solar-sail propulsion

To model the solar-sail acceleration, this paper will consider both an ideal and an optical solar-sail reflectance model. Considering both these models will allow to compute not only the theoretically fastest trajectory possible (for the ideal model) but also a more realistic trajectory (for the optical model). While the ideal model assumes the sail to be a perfect, specular reflector, the optical model also includes the effects of absorption, diffuse reflection and thermal emission. Though different in performance, both solar-sail models can be captured in the mathematical definition provided below.

The solar-sail acceleration vector can be decomposed into a component normal to the sail, $a_n \hat{\mathbf{n}}$, and a component tangential to the sail, $a_t \hat{\mathbf{t}}$, see Figure 3:

$$\mathbf{a}_s = a_n \hat{\mathbf{n}} + a_t \hat{\mathbf{t}} = a_s \hat{\mathbf{m}}. \tag{4}$$

The normal to the sail, $\hat{\mathbf{n}}$, can be defined through two angles, the solar-sail pitch and clock angles, that define the solar sail's orientation with respect to the direction of sunlight, see Figure 4. For this, a new reference frame $S(\hat{\mathbf{r}}_1, \hat{\boldsymbol{\theta}}_1, \hat{\boldsymbol{\varphi}}_1)$ is defined where the $\hat{\mathbf{r}}_1$-unit vector is directed along the Sun-sail line (see also below Eq. (3)) and the two remaining axes are defined as in Figure 4 (left schematic). The pitch angle, α, is then defined as the angle between the normal vector, $\hat{\mathbf{n}}$, and $\hat{\mathbf{r}}_1$, and the clock angle, δ, is defined as the

angle between the projection of $\hat{\mathbf{n}}$ onto the $\left(\hat{\boldsymbol{\theta}}_1, \hat{\boldsymbol{\varphi}}_1\right)$-plane and $\hat{\boldsymbol{\varphi}}_1$. This gives the following definition of the normal vector with respect to frame $S\left(\hat{\mathbf{r}}_1, \hat{\boldsymbol{\theta}}_1, \hat{\boldsymbol{\varphi}}_1\right)$:

$$\mathbf{n}\big|_{S\left(\hat{\mathbf{r}}_1, \hat{\boldsymbol{\theta}}_1, \hat{\boldsymbol{\varphi}}_1\right)} = \begin{bmatrix} \cos\alpha \\ \sin\alpha\sin\delta \\ \sin\alpha\cos\delta \end{bmatrix}. \tag{5}$$

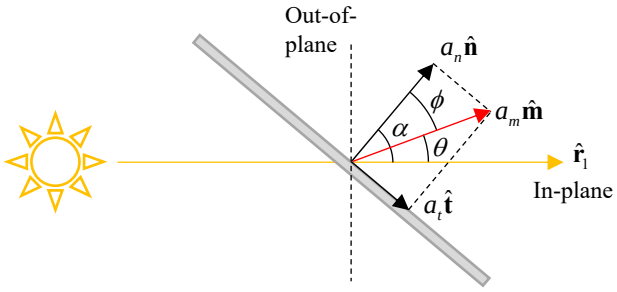

Figure 3. Side-view schematic of non-ideal solar-sail acceleration components.

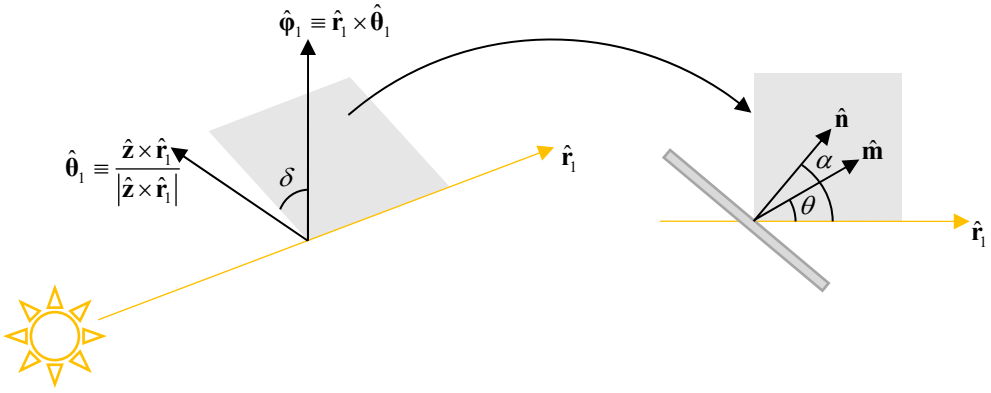

Figure 4. Solar-sail pitch and clock angles defined with respect to frame $S\left(\hat{\mathbf{r}}_1, \hat{\boldsymbol{\theta}}_1, \hat{\boldsymbol{\varphi}}_1\right)$ (adapted from Reference [20]).

Note that, due to the solar sail's inability to generate an acceleration component in the direction of the Sun, the normal vector always points away from the Sun. This can be reflected through appropriate bounds on the pitch and clock angles:

$$\begin{aligned} 0^o \le \alpha \le 90^o \\ -180^o \le \delta \le 180^o \end{aligned}. \tag{6}$$

The magnitudes of the solar-sail acceleration components along the normal and tangential directions in Eq. (4) are given by:[1]

$$\begin{aligned} a_n &= \frac{1}{2}\beta\frac{1-\mu}{r_1^2}\left[\left(1+\tilde{r}s\right)\cos^2\alpha + B_f\left(1-s\right)\tilde{r}\cos\alpha + \left(1-\tilde{r}\right)\frac{\varepsilon_f B_f - \varepsilon_b B_b}{\varepsilon_f + \varepsilon_b}\cos\alpha\right] \\ a_t &= \frac{1}{2}\beta\frac{1-\mu}{r_1^2}\left(1-\tilde{r}s\right)\cos\alpha\sin\alpha \end{aligned}. \tag{7}$$

In Eq. (7), β is the solar-sail lightness number, $\tilde{r}$ is the reflectivity coefficient that indicates the fraction of reflected photons, and s indicates the fraction of photons that are *specularly* reflected, while the term $(1-s)$ indicates the fraction of photons that are *diffusely* reflected; B_f and B_b are the non-Lambertian coefficients of the front (subscript 'f') and back (subscript 'b') of the sail, and ε_f and ε_b are the corresponding emissivity coefficients. Values for these optical coefficients for both an ideal sail and an optical sail model appear in Table 2. The optical sail coefficients have recently been obtained for NASA's proposed Near Earth Asteroid (NEA) Scout mission.[21] Finally, note that, by substituting the values for the ideal sail model into Eq. (7), only an acceleration component normal to the sail remains, i.e., $a_t = 0$ and therefore $\mathbf{a}_s = a_n\hat{\mathbf{n}}$ and $\hat{\mathbf{m}} = \hat{\mathbf{n}}$. From Eq. (7), the resulting acceleration direction, $\hat{\mathbf{m}}$, can be computed by first defining an auxiliary angle, ϕ, see Figure 3:[1]

$$\phi = \tan^{-1}\left(\frac{a_t}{a_n}\right) \tag{8}$$

such that

$$\theta = \alpha - \phi. \tag{9}$$

The direction of $\hat{\mathbf{m}}$ with respect to frame $S\left(\hat{\mathbf{r}}_1, \hat{\boldsymbol{\theta}}_1, \hat{\boldsymbol{\varphi}}_1\right)$ can then be defined as:

$$\hat{\mathbf{m}}\big|_{S\left(\hat{\mathbf{r}}_1,\hat{\boldsymbol{\theta}}_1,\hat{\boldsymbol{\varphi}}_1\right)} = \begin{bmatrix} \cos\theta \\ \sin\theta\sin\delta \\ \sin\theta\cos\delta \end{bmatrix}. \tag{10}$$

Through a transformation matrix, this normal vector can be transformed to the synodic Sun-Earth frame $B_{SE}\left(x_{SE}, y_{SE}, z_{SE}\right)$ for use in Eq. (4):

$$\hat{\mathbf{m}} = R_{S\to B_{SE}}\,\hat{\mathbf{m}}\big|_{S\left(\hat{\mathbf{r}}_1,\hat{\boldsymbol{\theta}}_1,\hat{\boldsymbol{\varphi}}_1\right)},\quad R_{S\to B_{SE}} = \begin{bmatrix} \hat{\mathbf{r}}_1 & \hat{\boldsymbol{\theta}}_1 & \hat{\boldsymbol{\varphi}}_1 \end{bmatrix}. \tag{11}$$

Table 2. Optical coefficients for an ideal and optical solar-sail reflectance model.

Reflectance model	$\tilde{r}$	s	B_f	B_b	ε_f	ε_b
Ideal	1	1	n/a	n/a	n/a	n/a
Optical[21]	0.91	0.94	0.79	0.67	0.025	0.27

Solar Electric Propulsion

In case of employing solar electric propulsion, the low-thrust acceleration vector in Eq. (2) is defined as

$$\mathbf{a} = \mathbf{a}_T = \frac{\mathbf{T}}{m}, \tag{12}$$

where $\mathbf{T} = \begin{bmatrix} T_x & T_y & T_z \end{bmatrix}^T$ is the Cartesian SEP thrust vector and m is the spacecraft mass. The SEP thrust vector direction can be defined in a similar way as the solar-sail normal vector using the pitch and clock angles, α_T and δ_T, respectively:

$$\mathbf{T}\big|_{S\left(\hat{\mathbf{r}}_1,\hat{\boldsymbol{\theta}}_1,\hat{\boldsymbol{\varphi}}_1\right)} = T\begin{bmatrix}\cos\alpha_T\\ \sin\alpha_T\sin\delta_T\\ \sin\alpha_T\cos\delta_T\end{bmatrix},\ \mathbf{T} = R_{S\to B_{SE}}\,\mathbf{T}\big|_{S\left(\hat{\mathbf{r}}_1,\hat{\boldsymbol{\theta}}_1,\hat{\boldsymbol{\varphi}}_1\right)} \tag{13}$$

with T the SEP thrust magnitude. Note that this time no restrictions need to be imposed on the pitch angle:

$$\begin{aligned} 0^o \le \alpha_T \le 180^o \\ -180^o \le \delta_T \le 180^o \end{aligned}. \tag{14}$$

Finally, due to the consumption of propellant, the spacecraft mass decreases over time according to

$$\dot{m} = -\frac{T}{I_{sp}g_0} \tag{15}$$

with I_{sp} = 1,600 s the assumed SEP thruster's specific impulse, see page 4, and g_0 the Earth's standard free fall constant. The differential equation in Eq. (15) needs to be integrated simultaneously with the spacecraft dynamics in Eq. (2).

Ballistic Earth-Moon phase

As highlighted in the mission assumptions section, the first phase of the trajectory is assumed to be ballistic (no use of the solar sail or SEP thruster) and is modelled in the Earth-Moon CR3BP. The dynamics are then as defined in Eq. (2), only now in the $B_{EM}\left(x_{EM},y_{EM},z_{EM}\right)$-frame with the Earth and Moon as primaries ($\mu = 0.01215$) and $\mathbf{a} = \mathbf{0}$. When integrating the dynamics forward from Eq. (1) up to the sphere of influence of the Earth (at a distance of 1,496,513 km), the trajectory in Figure 5 is obtained. It takes the spacecraft 9 days to reach the sphere of influence. Transforming the end of the trajectory to the inertial frame $A\left(X_I,Y_I,Z_I\right)$ and the synodic Sun-Earth frame $B_{SE}\left(x_{SE},y_{SE},z_{SE}\right)$, results in the conditions as shown in Figure 6. In the inertial frame, the conditions at the SOI oscillate around the orbit of the Earth and complete one revolution in one year, whereas in the synodic Sun-Earth frame, these conditions conduct one revolution per synodic lunar month.

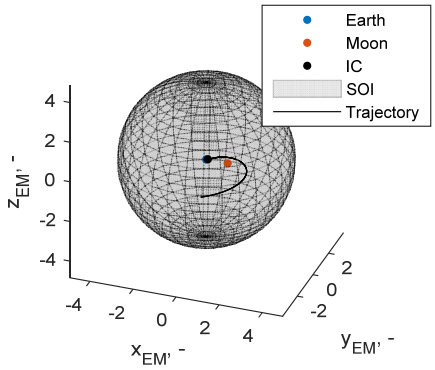

Figure 5. Ballistic trajectory starting from the initial condition in Eq. (1) depicted in the synodic Earth-Moon frame $B_{EM}\left(x_{EM},y_{EM},z_{EM}\right)$.

a) b)

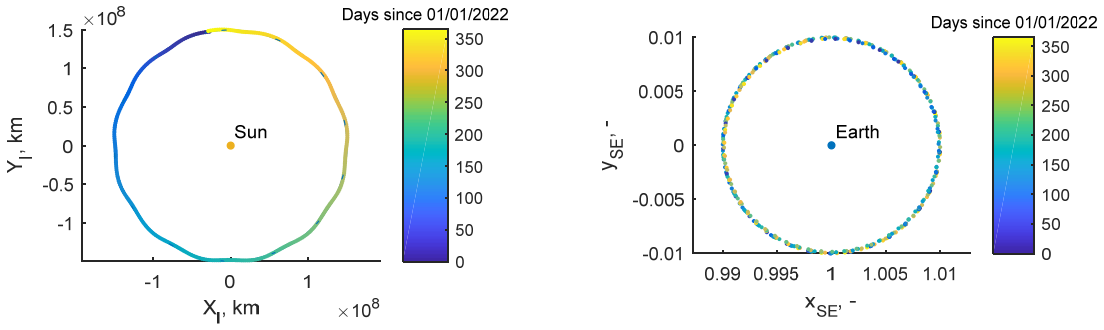

Figure 6. Conditions at Earth's sphere of influence of the trajectory in Figure 5 for the year 2022. a) In the inertial frame $A(X_I, Y_I, Z_I)$. b) In the synodic Sun-Earth frame $B_{SE}(x_{SE}, y_{SE}, z_{SE})$.

OPTIMAL CONTROL PROBLEM

Depending on the low-thrust propulsion system employed, the objective in this study is to either minimize the time of flight in the interplanetary part of the trajectory (for the solar-sail configuration) or the propellant consumption (for the SEP configuration). The objective, J, can thus be defined as

$$J = \begin{cases} t_f - t_0 & \text{Solar sail} \\ -m_f & \text{SEP} \end{cases}, \tag{16}$$

where t_0 and t_f are the initial and final time in the interplanetary phase and m_f is the final spacecraft mass. The goal then is to find the states, $\mathbf{x}(t)$, and controls, $\mathbf{u}(t)$, that minimize Eq. (16) and satisfy the dynamics in Eq. (2) as well as a set of boundary and path constraints.

The states are the position and velocity vectors in the CR3BP. For the SEP configuration, the spacecraft mass is added:

$$\mathbf{x}(t) = \begin{cases} \begin{bmatrix} \mathbf{r} & \dot{\mathbf{r}} \end{bmatrix}^T & \text{Solar sail} \\ \begin{bmatrix} \mathbf{r} & \dot{\mathbf{r}} & m \end{bmatrix}^T & \text{SEP} \end{cases}, \tag{17}$$

where the initial state, $\mathbf{x}(t_0) = \mathbf{x}_0$, needs to match the state vector at the end of the ballistic Earth-Moon phase at time t_0 and the final state, $\mathbf{x}(t_f) = \mathbf{x}_f$, needs to coincide with the asteroid's state vector at time t_f. Furthermore, for the SEP configuration, the initial mass is fixed to a value in the range $m_0 = 14$ – 21 kg, see page 4, and the final spacecraft mass is free, i.e., is to be optimized. Note that both the state vectors at the end of the ballistic phase and of the asteroid are computed in the optimization routine through an interpolation of large state matrices. Furthermore, suitable bounds need to be imposed on the state vector components:

$$\begin{bmatrix} (1-\mu)-0.4 & -0.6 & -0.4 & -0.5 & -0.5 & -0.5 & 0 \end{bmatrix}^T \le \mathbf{x}(t) \le \begin{bmatrix} (1-\mu)+0.4 & 0.6 & 0.4 & 0.5 & 0.5 & 0.5 & m_0 \end{bmatrix}^T, \tag{18}$$

where the last row in the vectors only applies to the SEP case.

The controls are also defined differently for the two low-thrust propulsion configurations:

$$\mathbf{u}(t) = \begin{cases} \begin{bmatrix} \alpha & \delta \end{bmatrix}^T & \text{Solar sail} \\ \begin{bmatrix} \alpha_T & \delta_T & T \end{bmatrix}^T & \text{SEP} \end{cases}, \tag{19}$$

where the following bounds are imposed:

$$\left.\begin{matrix} \begin{bmatrix} 0 & -\pi \end{bmatrix}^T \\ \begin{bmatrix} 0 & -\pi & 0 \end{bmatrix}^T \end{matrix}\right\} \mathbf{u}(t) = \begin{cases} \begin{bmatrix} \frac{1}{2}\pi & \pi \end{bmatrix}^T & \text{Solar sail} \\ \begin{bmatrix} \pi & \pi & T_{\max} \end{bmatrix}^T & \text{SEP} \end{cases}. \tag{20}$$

In Eq. (20), $T_{\max} = 0.9$ mN is the assumed maximum thrust magnitude, see page 4. In addition, a path constraint is included to avoid close Earth approaches:

$$r_2(t) \geq 800{,}000 \text{ km}. \tag{21}$$

Finally, bounds on the initial and final time need to be specified to ensure a launch in the assumed 2022 – 2023 launch window and to limit the search space on the final time:

$$\begin{aligned} \text{1 January 2022} \leq t_0 \leq \text{ 31 December 2023} \\ \text{31 December 2023} \leq t_f \leq \text{ 1 January 2028} \end{aligned} \tag{22}$$

Note that the time in the actual implementation of the optimal control problem is defined in non-dimensional units after 1 January 2022, i.e., 1 January 2022 is represented by $t = 0$, 1 January 2023 is represented by $t = 2\pi$, and so on.

The optimal control problem defined in Eqs. (16)-(22) is solved with a particular implementation of a direct pseudospectral method in C^{++}, PSOPT.[18] PSOPT is an open source tool developed by Victor M. Becerra of the University of Reading, UK. It can use both Legendre and Chebyshev polynomials to approximate and interpolate the dependent variables at the nodes. However, in this work, only the Legendre pseudospectral method is used and PSOPT is interfaced to the NLP solver IPOPT (Interior Point OPTimizer), an open source C^{++} implementation of an interior point method for large scale problems.[22] Furthermore, a consecutive mesh refinement of [50,75,100] nodes is applied, a convergence tolerance of 10^{-6} is used and a maximum number of iterations per mesh refinement of 1000 is enforced.

INITIAL GUESS

In order to initiate the optimization process, PSOPT requires an initial guess of the states, controls and time, which are constructed through the following approach:

- First, the launch date, t_L, and the pitch and clock angles, (α, δ) or (α_T, δ_T), are fixed. Furthermore, for the solar-sail case, the sail lightness number, β, is fixed whereas for the SEP case the thrust magnitude is set to its maximum value, $T_{\max}$.
- Subsequently, the initial condition in Eq. (1) is forward integrated from t_L up to the sphere of influence to construct the ballistic Earth-Moon phase and the end of the trajectory is transformed to the $B_{SE}(x_{SE}, y_{SE}, z_{SE})$ frame.
- Then, the integration is continued to construct the interplanetary phase, where the low-thrust acceleration is defined by either (α, δ, β) or $(\alpha_T, \delta_T, T_{\max})$. The integration is truncated after 5

years. In addition, to aid the trajectory in increasing its inclination to that of the asteroid, a rudimentary out-of-plane steering law is adopted where the out-of-plane component of the acceleration takes the sign of the $y-$coordinate. For example, for the solar-sail case:

$$\hat{\mathbf{m}} = \begin{cases} \begin{bmatrix} m_x & m_y & |m_z| \end{bmatrix}^T & y \geq 0 \\ \begin{bmatrix} m_x & m_y & -|m_z| \end{bmatrix}^T & y < 0 \end{cases} \tag{23}$$

and similar for $\mathbf{T}$ for the SEP case.

- Subsequently, at each time step in the propagated trajectory, t, that occurs after 3 years of flight, the *dimensionless* error in distance, Δr, and error in velocity, ΔV, between the spacecraft's state-vector and that of the asteroid is computed.
- Finally, the trajectory is truncated at the point where the sum of these errors, $\Delta r + \Delta V$, is minimal. Note that, in dimensionless units, a position error of 5000 km and a velocity error of 1 m/s are of the same order of magnitude.

For a given performance of the solar-sail or SEP configuration, i.e., for a given value for β or $T_{\max}$, the trajectory is fully defined by the following set of three parameters:

$$\mathbf{p} = \begin{cases} \begin{bmatrix} t_L & \alpha & \delta \end{bmatrix} & \text{Solar sail} \\ \begin{bmatrix} t_L & \alpha_T & \delta_T \end{bmatrix} & \text{SEP} \end{cases}, \tag{24}$$

which define the objective

$$J(\mathbf{p}) = \Delta r + \Delta V . \tag{25}$$

To find the values for the parameters in Eq. (24) that minimize the objective in Eq. (25), a genetic algorithm is employed. In particular, the Matlab® function *ga.m* is used with 1000 individuals and a maximum of 50 generations while enforcing the following bounds on the optimization parameters:

$$\left.\begin{matrix} \begin{bmatrix} 1-1-2022 & 0 & -\pi \end{bmatrix} \\ \begin{bmatrix} 1-1-2022 & 0 & -\pi \end{bmatrix} \end{matrix}\right\} \leq \mathbf{p} \leq \begin{cases} \begin{bmatrix} 31-12-2023 & \frac{1}{2}\pi & \pi \end{bmatrix} & \text{Solar sail} \\ \begin{bmatrix} 31-12-2023 & \pi & \pi \end{bmatrix} & \text{SEP} \end{cases} .$$

Finally, note that, to account for the inherent randomness of the genetic algorithm approach, each simulation case is run for five different seed values.

Solar-sail initial guesses

Solar-sail initial guesses are generated for both the ideal and optical sail models and for four different lightness numbers, $\beta = [0.025, 0.03, 0.035, 0.04]$, to cover the assumed lightness number range, see page 4. For each lightness number, the genetic algorithm is run five times (for the five different seed values), resulting in a total of 20 runs per sail model. The best trajectory for each lightness number, i.e., the trajectory with the smallest objective function value among the five runs, appears in Figure 7 (for an ideal sail model) with numerical values in Table 3 (for both sail models). From these results, the following observations can be made:

- The larger the lightness number, the smaller the objective function value (8th column in Table 3), which indicates that the rendezvous conditions at the asteroid can be more easily met with better solar-sail technology.

- No clear favorable "launch window" can be deduced from the launch dates in Table 3, though from all results (i.e., from all 20 runs per sail model) a clear preference for launch in January, February, June, July, and October (of either 2022 or 2023) can be observed. None of the optimized results showed a launch in spring (March – May). Finally, there is no clear preference for launch in 2022 or 2023. These observations show that the problem at hand most likely contains many local minima, with multiple suitable launch dates in the time frame 2022 – 2023.
- The optimal value for the solar-sail pitch angle is in the approximate range of 30 – 40 deg, while the clock angle is close to zero or 180 depending on whether "rendezvous" takes place closer to the asteroid's ascending or descending node, respectively.
- Finally, due to the limited number of controls (especially the constant pitch and clock angles throughout the trajectory), a mismatch in position and significant mismatch in velocity still exist between the spacecraft and asteroid at the end of the trajectory. These errors can, however, be overcome by the optimizer.

SEP initial guesses

For the SEP case, initial guesses are generated for the extremes of the range in initial spacecraft mass: $m_0 = 14$ kg and $m_0 = 21$ kg, see page 4. Similar to the initial guesses for the solar-sail case, five runs (for the five different seed values) are conducted for each initial mass. The best trajectories for each value for m_0 appear in Figure 8 with numerical values in Table 4. From these results, the following observations can be made:

- The arrival date for nearly all generated initial guesses occurs in the months June and November, when the asteroid is at one of its nodal crossings in the years 2025 – 2027.
- Contrary to the solar-sail case, out-of-plane thrusting is barely exploited: the pitch and clock angles are close to 90 deg, indicating that thrusting takes place entirely in the ecliptic plane and along the $y_{SE}-$axis. Apparently, this thrusting law provided the smallest combined error on the position and velocity with the asteroid at the end of the trajectory. As Figure 8 and Table 4 clearly show, while this leads to relatively small errors on the position, large errors on the velocity remain.
- Finally, due to the assumption of continuous thrusting at the maximum thrust magnitude, the propellant consumption is large: 6.93 kg and 7.47 kg for $m_0 = 14$ kg and $m_0 = 21$ kg, respectively. This greatly exceeds the expected propellant budget of 1.5 kg, see page 4.

RESULTS

Due to the assumed wide launch window (2022 – 2023), the problem at hand contains many local minima. This already became apparent in the results for the initial guess in the previous section. It can therefore be expected that PSOPT will converge to a different local minimum when provided with a different initial guess. To therefore best detect the global minimum, PSOPT is run for each generated initial guess, i.e., not only for the best initial guesses that appear in Table 3, but for all 40 (solar-sail case) and 10 (SEP case) generated initial guesses. The results of the runs that generated the best trajectory in terms of objective function value (i.e., the total time of flight) are presented in this section.

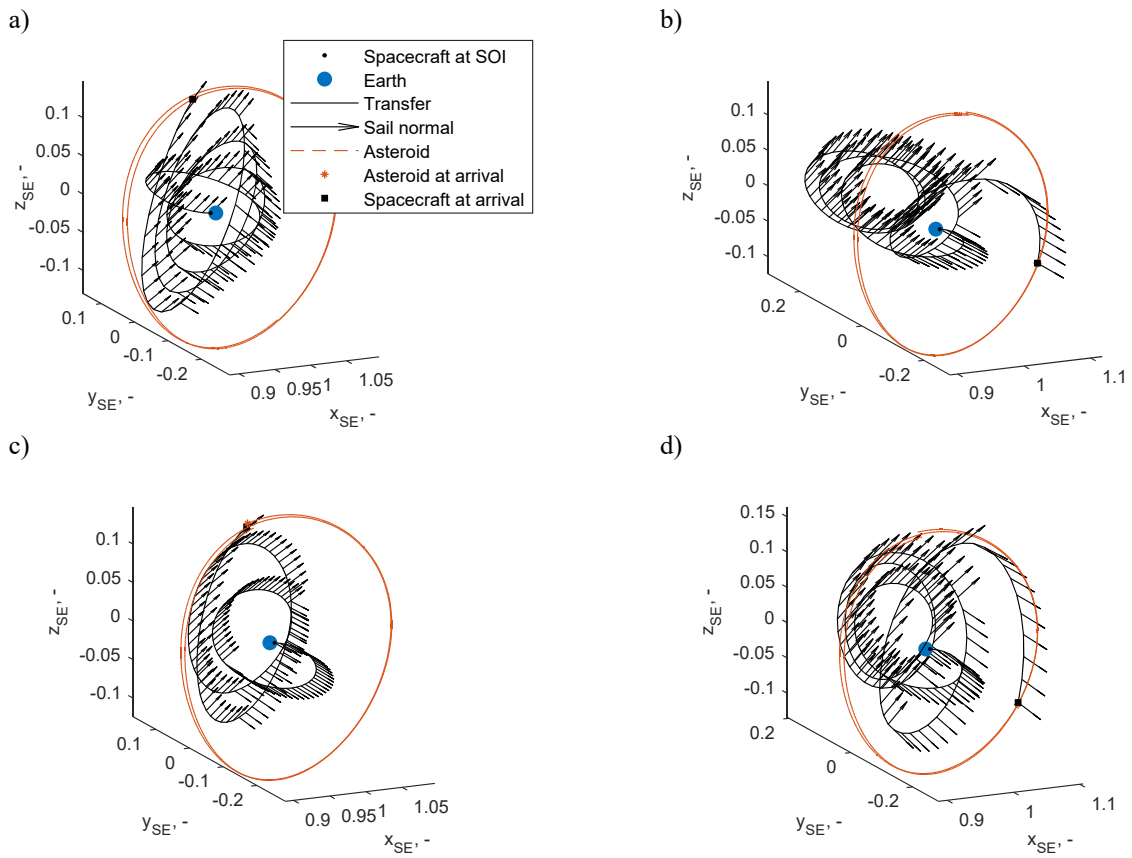

Figure 7. Solar-sail case – best initial guess trajectories in the synodic Sun-Earth frame $B_{SE}\left(x_{SE}, y_{SE}, z_{SE}\right)$ for an ideal solar-sail model and for a) $\beta = 0.025$, b) $\beta = 0.03$, c) $\beta = 0.035$, and d) $\beta = 0.04$.

Table 3. Solar-sail case - details of best initial guesses.

	β	Launch date	Arrival date	Time of flight, Δt, yrs	Pitch angle, α, deg	Clock angle, δ, deg	J	Δr, km	ΔV, km/s
Ideal sail model	**0.025**	10 July 2022	16 Jan 2027	4.51	40.65	-4.17	0.0710	6,600	2.114
	0.03	15 Feb 2023	3 June 2027	4.29	31.82	5.76	0.0693	53,357	2.053
	0.035	17 Jan 2023	19 Jan 2026	3.00	33.38	179.90	0.0580	773,675	1.575
	0.04	25 Jan 2022	15 June 2026	4.37	38.97	178.93	0.0451	418,300	1.261
Optical sail model	**0.025**	17 Jan 2023	22 June 2027	4.41	34.67	178.60	0.0863	3,394,765	1.895
	0.03	10 July 2022	12 Jan 2027	4.50	28.16	-4.23	0.0695	43,830	2.060
	0.035	25 Jan 2022	8 July 2025	3.44	33.17	177.26	0.0612	155,470	1.791
	0.04	25 Feb 2022	11 June 2026	4.28	39.44	174.38	0.0559	1,105,868	1.444

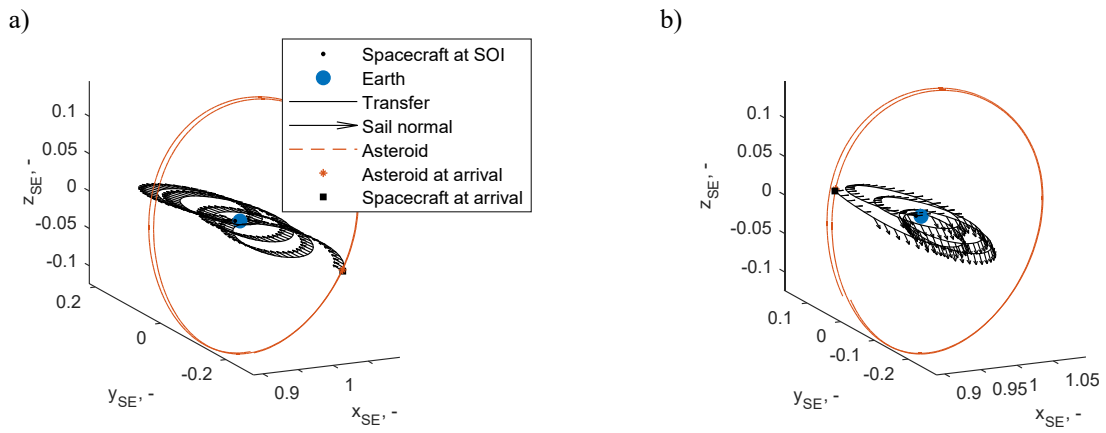

Figure 8. SEP case – best initial guess trajectories in the synodic Sun-Earth frame $B_{SE}\left(x_{SE}, y_{SE}, z_{SE}\right)$ for a) m_0 = 14 kg and b) m_0 = 21 kg.

Table 4. SEP case - details of best initial guesses.

m_0	Launch date	Arrival date	Time of flight, Δt, yrs	Propellant mass, kg	Pitch angle, α_T, deg	Clock angle, δ_T, deg	J	Δr, km	ΔV, km/s
14	9 Aug 2022	10 June 2026	3.83	6.93	100.89	90.92	0.1467	684,804	4.2334
21	7 Oct 2022	26 Nov 2026	4.12	7.47	97.00	-74.19	0.1568	521,778	4.5662

Solar-sail optimal results

The results for each considered value for the solar-sail lightness number appear in Table 5 for both the ideal and optical sail models with details for a subset of the results in Figure 9 and Figure 10 for $\beta = 0.025$ and $\beta = 0.04$, respectively. Note that the clock angle profiles in Figure 9 and Figure 10 may appear erratic, but a clock angle switch from $-\pi$ to π does not require an actual physical change in the solar-sail attitude.

Table 5. Solar-sail case – optimized results.

	Ideal sail model			Optical sail model			
β	Launch date	Arrival date	Time of flight, Δt, yrs	Launch date	Arrival date	Time of flight, Δt, yrs	Difference in Δt between sail models, %
0.025	7 Oct 2022	10 Apr 2026	3.51	16 Mar 2023	1 June 2027	4.21	19.9
0.03	15 Feb 2023	15 Jan 2026	2.92	24 Feb 2022	3 Aug 2025	3.44	17.8
0.035	15 Feb 2023	19 Aug 2025	2.51	7 Oct 2022	9 Oct 2025	3.01	19.9
0.04	8 Oct 2022	3 Dec 2024	2.16	9 Oct 2022	11 May 2025	2.59	19.9

From the results in Table 5, Figure 9, and Figure 10, the following observations can be made:

- PSOPT is able to overcome the discontinuities in the state vector of the initial guess at the end of the trajectory between the sailcraft and the asteroid, while decreasing the time of flight compared to the initial guess by (on average) 1.4 and 0.7 years for the ideal and optical sail models, respectively.

- The best initial guess as in Table 3 does not necessarily lead to the best optimized result. In fact, only for an ideal sail model and a lightness number of $\beta = 0.03$ did the best initial guess provide the best optimized result.
- The difference in launch date between the initial guess and the corresponding optimized trajectory is, on average, only 2 days. This implies that the reduction in time of flight is only due to an advancement of the arrival date, not due to a change in launch date. For example, for the case of an ideal sail model and $\beta = 0.03$ the launch date of both the initial guess and the optimized trajectory is 15 February 2022, while the time of flight is 1.4 years shorter, see Table 3 and Table 5. The underlying reason can be found in the fact that the launch conditions change much more rapidly over time than the arrival conditions (see above Figure 5). The optimizer therefore shies away from altering the launch conditions and prefers to change the arrival conditions.
- The ideal sail model provides the absolute fastest trajectory possible, which ranges from 2.16 – 3.54 years for lightness numbers in the range 0.025 – 0.04. The optical sail model presents a more realistic performance of the sail, but increases the time of flight by 17.8 – 19.9 percent to 2.59 – 4.21 years.

SEP optimal results

Following the same approach as for the solar-sail optimal results, minimum-propellant trajectories can be generated for the nominal SEP case, which appear in the first two rows of Table 6 with details for $m_0 = 14$ kg in Figure 11. The table shows that two additional cases have been considered with larger specific impulses and maximum thrust magnitudes. These results will be discussed later.

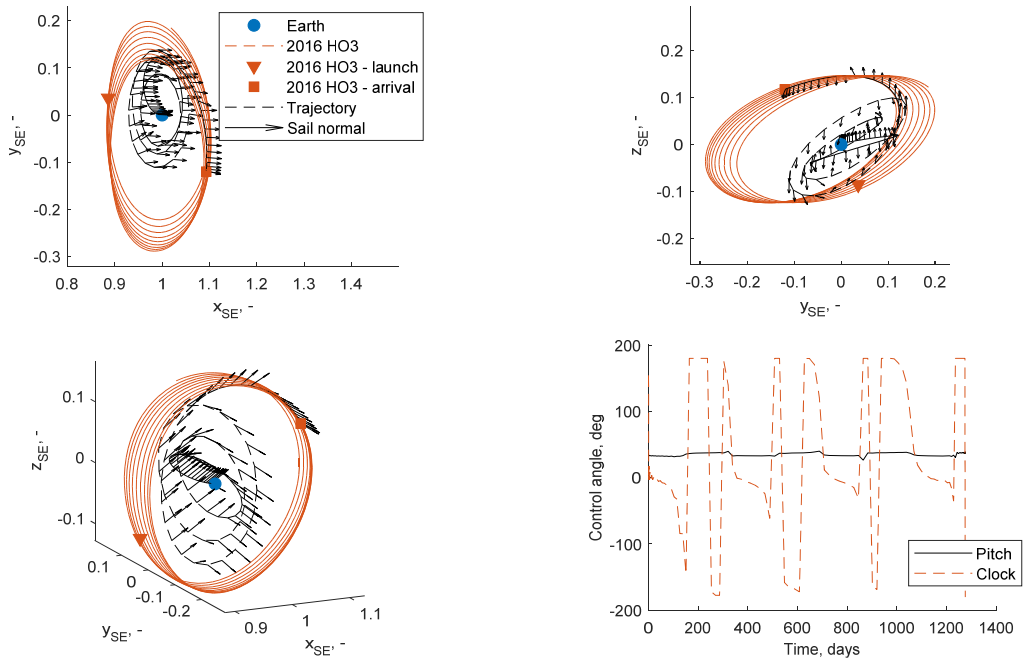

Figure 9. Solar-sail case – optimized trajectory and controls for ideal sail model and $\beta = 0.025$.

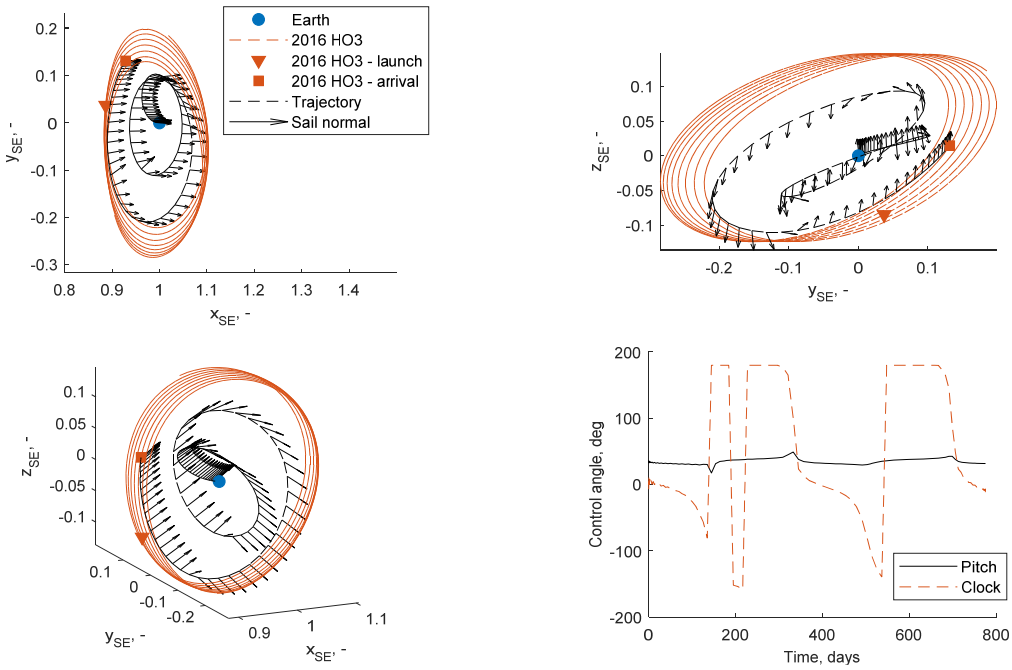

Figure 10. Solar-sail case – optimized trajectory and controls for ideal sail model and $\beta = 0.04$.

Table 6. SEP case - minimum-propellant results.

Case	m_0, kg	I_{sp}, s	T_{max}, mN	Launch date	Arrival date	Propel-lant mass, kg	Time of flight, yrs	Thruster operating time, hrs
1	14	1,600	0.9	8 Aug 2022	24 Dec 2026	3.60	4.38	15,814
2	21	1,600	0.9	6 Oct 2022	19 May 2027	5.90	4.62	25,616
3	14	2,100	1.15	5 Oct 2022	12 Feb 2026	2.91	3.36	13,966
4	21	2,100	1.15	5 Oct 2022	16 Dec 2026	4.51	4.20	21,054

From the results in the first two rows of Table 6 and Figure 11, the following observations can be made:

- PSOPT is again able to overcome the discontinuities in the state vector of the initial guess at the end of the trajectory between the spacecraft and the asteroid, while this time decreasing the propellant consumption compared to the initial guess to 3.60 kg and 5.90 kg for $m_0 = 14$ kg and $m_0 = 21$ kg, respectively. However, again considering the expected maximum on-board propellant capacity of 1.5 kg (see page 4), all trajectories appear infeasible from that point of view.
- The decrease in propellant consumption (and matching of the rendezvous constraints) comes at a cost in an increase in the time of flight compared to the initial guess of approximately 0.5 year: to 4.38 years and 4.62 years for $m_0 = 14$ kg and $m_0 = 21$ kg, respectively. These times of flight exceed the maximum thruster operation duration of 20,000 hours or 2.3 years. However, when only considering the time that thrust is actually produced, this reduces to 15,814 and 25,616 hours for $m_0 = 14$ kg and $m_0 = 21$ kg, respectively, where the former does satisfy the constraint. Finally, also note that these times of flight are all longer than the times of flight obtained for the solar-sail case. Here, it must be noted that the solar-sail cases were optimized for the time of flight, while the SEP case is only optimized for the propellant consumption. Therefore, when changing the objective function in Eq. (16) for the SEP case to the time of flight, shorter transfers are obtained (2.58

years and 3.87 years for $m_0 = 14$ kg and $m_0 = 21$ kg, respectively). However, this comes at the cost of a significant increase in the propellant consumption that further violates the constraint on the propellant capacity (4.65 kg and 6.96 kg for $m_0 = 14$ kg and $m_0 = 21$ kg, respectively) and thruster operating times that far exceed the maximum duration (22,520 hours and 33,745 hours for $m_0 = 14$ kg and $m_0 = 21$ kg, respectively).

- Similar conclusions as for the solar-sail case can be drawn regarding the fact that the best initial guess as in Table 3 does not necessarily lead to the best optimized result and that the launch date does not change much (if at all) with respect to the initial guess.

From the observations listed above, it can be concluded that solar electric propulsion (under the assumptions on page 4) does not seem a viable propulsion method for this mission, both from a propellant consumption point of view, thruster operating times and flight-time. To further support this conclusion, additional simulations have been conducted for an even better-performing SEP system (see the results in the last two rows in Table 6). Here, the specific impulse has been increased to $I_{sp} = 2{,}100$ s and the maximum thrust magnitude to $T_{\max} = 1.15$ mN, the maximum value as specified in Reference 19. The results in Table 6 show that these improvements lower the propellant consumption and the thruster operation duration. However, the propellant consumption is still larger than the expected budget of 1.5 kg and the thruster operation duration is still too long for $m_0 = 21$ kg. Finally, while the times of flight are also reduced, they are still longer than those for the solar-sail trajectories for $\beta > 0.025$ (ideal sail) and $\beta > 0.03$ (optical sail).

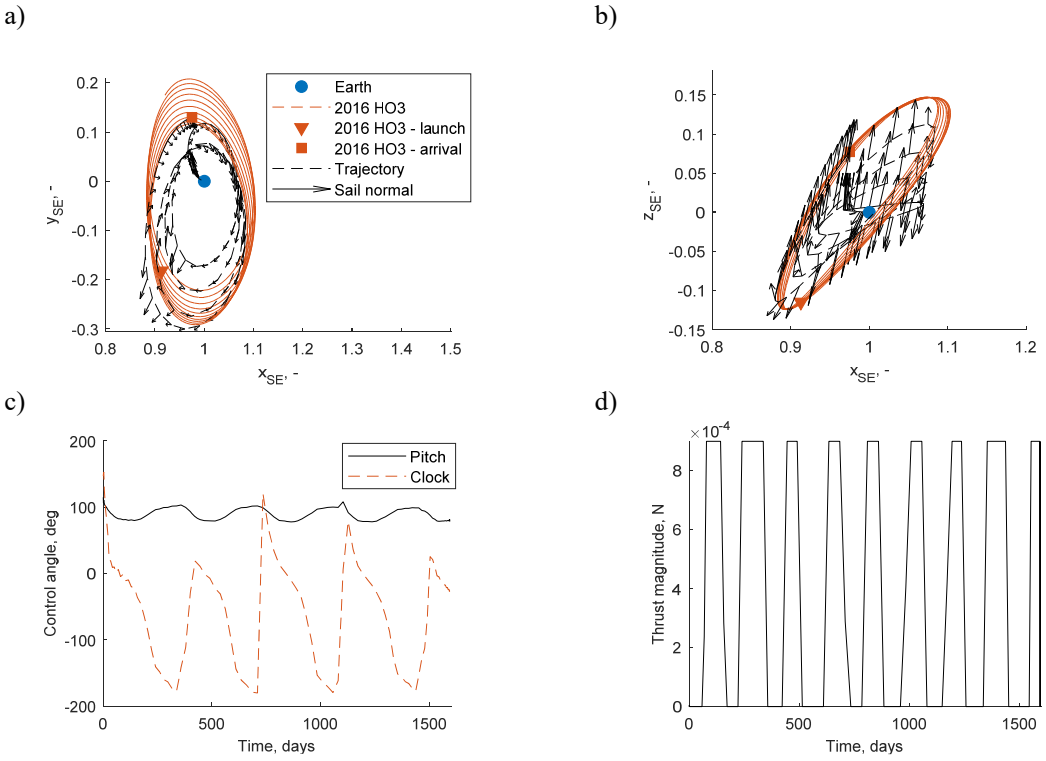

Figure 11. SEP case - minimum-propellant results for case 1: m_0 = 14 kg, I_{sp} = 1,600 s, and $T_{\max}$ = 0.9 mN. a) Trajectory projected onto the ecliptic plane. b) Trajectory in the out-of-plane direction. c) Thrust angles. d) Thrust magnitude.

CONCLUSIONS

This paper has presented minimum-time solar-sail trajectories and minimum-propellant solar electric propulsion (SEP) trajectories for a CubeSat mission to asteroid 2016 HO_3 within a set of mission assumptions. In particular, the trajectory is assumed to start from a fixed state in the Earth-Moon system, followed by a ballistic arc up to the Earth's sphere of influence, after which the low-thrust propulsion system is activated to rendezvous with 2016 HO_3. For the solar-sail configuration, trajectories take 2.16 – 3.51 years for lightness numbers in the range 0025 – 0.04 (with shorter flight times for larger lightness numbers) if the solar sail acts as a perfectly reflecting mirror. If slight optical imperfections are included in the solar-sail reflectance model, these times of flight increase by approximately 20 percent to 2.59 – 4.21 years. For the assumed nominal SEP thruster performance, times of flight of 4.38 years and 4.62 years are obtained for spacecraft initial masses of 14 kg and 21 kg, respectively, which is longer than any solar-sail case considered. Furthermore, the trajectories require propellant consumptions of 3.60 kg and 5.90 kg, which exceed the expected available onboard propellant mass capacity of 1.5 kg. Finally, the required thruster operation duration for an initial mass of 14 kg exceeds the expected maximum operating duration of 20,000 hours. When pushing the SEP technology to its maximum (assuming a larger specific impulse and maximum thrust magnitude), smaller propellant consumptions are obtained (though still beyond the available 1.5 kg) as well as shorter times of flight, though still not as fast as the solar-sail trajectories with lightness number larger than 0.025 (ideal sail) or 0.03 (optical sail). From these analyses the superior capabilities of solar-sail technology for this mission seem to be evident.

ACKNOWLEDGMENTS

Jeannette Heiligers would like to acknowledge support from the Marie Skłodowska-Curie Individual Fellowship 658645 - S4ILS: Solar Sailing for Space Situational Awareness in the Lunar System.

REFERENCES

1. McInnes, C.R., "Solar Sailing: Technology, Dynamics and Mission Applications," *Springer-Praxis Books in Astronautical Engineering*, Springer-Verlag, Berlin, 1999.
2. Vulpetti, G., "Fast Solar Sailing," *Space Technology Library*, Vol. 30, Springer Science + Business Media, Dordrecht, 2013.
3. Kawaguchi, J.i., Fujiwara, A., and Uesugi, T., "Hayabusa - Its Technology and Science Accomplishment Summary and Hayabusa-2," *Acta Astronautica*; Vol. 62, No. 10–11, 2008, pp. 639-647. doi: 10.1016/j.actaastro.2008.01.028
4. Brophy, J.R., Etters, M.A., Gates, J., Garner, C.E., Klatte, M., Lo, C.J., Marcucci, M.G., Mikes, S., Pixler, G., and Nakazono, B., "Development and Testing of the Dawn Ion Propulsion System," *42nd AIAA/ASME/SAE/ASEE Joint Propulsion Conference & Exhibit*, AIAA-2006-4319, Sacramento, CA, USA, 2006.
5. Lewis, R.A., Pérez Luna, J., Coombs, N., and Guarducci, F., "Qualification of the T6 Thruster for BepiColombo," *Joint Conference of 30th International Symposium on Space Technology and Science, 34th International Electric Propulsion Conference, and 6th Nano-satellite Symposium*, Hyogo-Kobe, Japan, 2015.
6. McNutt, L., Johnson, L., Clardy, D., Castillo-Rogez, J., Frick, A., and Jones, L., "Near-Earth Asteroid Scout," *AIAA SPACE 2014 Conference and Exposition*, American Institute of Aeronautics and Astronautics, San Diego, CA, USA, 2014.
7. Macdonald, M., Hughes, G.W., McInnes, C.R., Lyngvi, A., Falkner, P., and Atzei, A., "Solar Polar Orbiter: A Solar Sail Technology Reference Study," *Journal of Spacecraft and Rockets*; Vol. 43, No. 5, 2006, pp. 960-972. doi: 10.2514/1.16408
8. West, J.L., "The GeoStorm Warning Mission: Enhanced Opportunities Based on New Technology," *14th AAS/AIAA Spaceflight Mechanics Conference*, AAS-04-102, Maui, HI, USA, 2004.

9. Heiligers, J., Diedrich, B., Derbes, B., and McInnes, C.R., "Sunjammer: Preliminary End-to-End Mission Design," *2014 AIAA/AAS Astrodynamics Specialist Conference*, San Diego, CA, USA, 2014.
10. Leipold, M., Fichtner, H., Heber, B., Groepper, P., Lascar, S., Burger, F., Eiden, M., Niederstadt, T., Sickinger, C., Herbeck, L., Dachwald, B., and Seboldt, W., "Heliopause Explorer - A Sailcraft Mission to the Outer Boundaries of the Solar System," *Acta Astronautica*; Vol. 59, 2006, pp. 785-796. doi: 10.1016/j.actaastro.2005.07.024
11. McKay, R.J., Macdonald, M., Biggs, J., and McInnes, C., "Survey of Highly Non-Keplerian Orbits with Low-Thrust Propulsion," *Journal of Guidance, Control, and Dynamics*; Vol. 34, No. 3, 2011. doi: 10.2514/1.52133
12. Heiligers, J. and McInnes, C., "Novel Solar Sail Mission Concepts for Space Weather Forecasting," *24th AAS/AIAA Space Flight Mechanics Meeting*, Santa Fe, NM, USA, 2014.
13. Heiligers, J. and Scheeres, D., "Solar Sail Orbital Motion About Asteroids and Binary Asteroid Systems," *Journal of Guidance, Control, and Dynamics*; Vol. Online, 2017. doi: 10.2514/1.G003235
14. Macdonald, M., Hughes, G., McInnes, C., A, L., Falkner, P., and Atzei, A., "GeoSail: An Elegant Solar Sail Demonstration Mission," *Journal of Spacecraft and Rockets*; Vol. 44, No. 4, 2007, pp. 784-796. doi: 10.2514/1.22867
15. Heiligers, J., Parker, J.S., and Macdonald, M., "Novel Solar-Sail Mission Concept for High-Latitude Earth and Lunar Observation," *Journal of Guidance, Control, and Dynamics*; Vol. 41, No. 1, 2018. doi: 10.2514/1.G002919
16. Ozimek, M.T., Grebow, D.J., and Howell, K.C., "Design of Solar Sail Trajectories with Applications to Lunar South Pole Coverage," *Journal of Guidance, Control, and Dynamics*; Vol. 32, No. 6, 2009, pp. 1884-1897. doi: 10.2514/1.41963
17. Fernandez, J.M., Rose, G., Stohlman, O.R., Younger, C.J., Dean, G.D., Warren, J.E., Kang, J.H., Bryant, R.G., and Wilkie, K.W., "An Advanced Composites-Based Solar Sail System for Interplanetary Small Satellite Missions," *2018 AIAA Spacecraft Structures Conference*, American Institute of Aeronautics and Astronautics, Kissimmee, FL, USA, Jan 8-12, 2018.
18. Becerra, V.M., "Solving Complex Optimal Control Problems at No Cost with PSOPT," *IEEE Multi-conference on Systems and Control*, Yokohama, Japan, 2010.
19. Busek Space Propulsion Systems. *BIT-3 RF Ion Thruster*. [cited December 9 2017]; Available from: http://www.busek.com/index_htm_files/70010819C.pdf.
20. Ceriotti, M. and McInnes, C.R., "Generation of Optimal Trajectories for Earth Hybrid Pole Sitters," *Journal of Guidance, Control, and Dynamics*; Vol. 34, No. 3, 2011, pp. 847-859. doi: 10.2514/1.50935
21. Heaton, A., Ahmad, N., and Miller, K., "Near Earth Asteroid Scout Solar Sail Thrust and Torque Model (17055)," *4th International Symposium on Solar Sailing*, Japan Space Forum, Kyoto, Japan, 2017.
22. Wächter, A. and Biegler, L.T., "On the Implementation of an Interior-point Filter Line-search Algorithm for Large-scale Nonlinear Programming," *Mathematical Programming*; Vol. 106, No. 1, 2006, pp. 25-57. doi: 10.1007/s10107-004-0559-y
23. Banik, J. A., Murphey, T. W., “Performance Validation of the Triangular Rollable And Collapsible Mast”, 24th Annual AIAA/USU Conference on Small Satellites, Logan, UT, August 2010. SSC10-II-1.
24. Betts, B., et al., “LightSail 2: Controlled Solar Sailing Using a CubeSat”, 4th International Symposium on Solar Sailing. Kyoto, Japan, 17-20 January 2017
25. Stohlman, O., Loper, E., Thermal deformation of very slender triangular rollable and collapsible booms , AIAA Scitech, San Diego, CA, 2016.
26. Stohlman, O., Loper, E., and Lockett, T., Temperature-driven shape changes of the Near Earth Asteroid Scout solar sail, 4th International Symposium on Solar Sailing, Kyoto, 2017